DESY 04-209
October 2004

ISSN 0418-9833

arXiv:hep-ex/0411046 v1 12 Nov 2004

Measurement of $F_2^{c\bar{c}}$ and $F_2^{b\bar{b}}$ at High Q^2 using the H1 Vertex Detector at HERA

H1 Collaboration

Abstract

Measurements are presented of inclusive charm and beauty cross sections in e^+p collisions at HERA for values of photon virtuality $Q^2 > 150\ \mathrm{GeV}^2$ and of inelasticity $0.1 < y < 0.7$. The charm and beauty fractions are determined using a method based on the impact parameter, in the transverse plane, of tracks to the primary vertex, as measured by the H1 vertex detector. The data are divided into four regions in Q^2 and Bjorken x, and values for the structure functions $F_2^{c\bar{c}}$ and $F_2^{b\bar{b}}$ are obtained. The results are found to be compatible with the predictions of perturbative quantum chromodynamics.

To be submitted to *Eur. Phys. J.* **C**

A. Aktas[10], V. Andreev[26], T. Anthonis[4], S. Aplin[10], A. Asmone[33], A. Babaev[25], S. Backovic[37], J. Bähr[37], A. Baghdasaryan[36], P. Baranov[26], E. Barrelet[30], W. Bartel[10], S. Baudrand[28], S. Baumgartner[38], J. Becker[39], M. Beckingham[10], O. Behnke[13], O. Behrendt[7], A. Belousov[26], Ch. Berger[1], N. Berger[38], T. Berndt[14], J.C. Bizot[28], J. Böhme[10], M.-O. Boenig[7], V. Boudry[29], J. Bracinik[27], G. Brandt[13], V. Brisson[28], H.-B. Bröker[2], D.P. Brown[10], D. Bruncko[16], F.W. Büsser[11], A. Bunyatyan[12,36], G. Buschhorn[27], L. Bystritskaya[25], A.J. Campbell[10], S. Caron[1], F. Cassol-Brunner[22], K. Cerny[32], V. Chekelian[27], J.G. Contreras[23], Y.R. Coppens[3], J.A. Coughlan[5], B.E. Cox[21], G. Cozzika[9], J. Cvach[31], J.B. Dainton[18], W.D. Dau[15], K. Daum[35,41], B. Delcourt[28], R. Demirchyan[36], A. De Roeck[10,44], K. Desch[11], E.A. De Wolf[4], C. Diaconu[22], J. Dingfelder[13], V. Dodonov[12], A. Dubak[27], C. Duprel[2], G. Eckerlin[10], V. Efremenko[25], S. Egli[34], R. Eichler[34], F. Eisele[13], M. Ellerbrock[13], E. Elsen[10], W. Erdmann[38], S. Essenov[25], P.J.W. Faulkner[3], L. Favart[4], A. Fedotov[25], R. Felst[10], J. Ferencei[10], L. Finke[11], M. Fleischer[10], P. Fleischmann[10], Y.H. Fleming[10], G. Flucke[10], G. Flügge[2], A. Fomenko[26], I. Foresti[39], J. Formánek[32], G. Franke[10], G. Frising[1], T. Frisson[29], E. Gabathuler[18], K. Gabathuler[34], E. Garutti[10], J. Garvey[3], J. Gayler[10], R. Gerhards[10,†], C. Gerlich[13], S. Ghazaryan[36], S. Ginzburgskaya[25], A. Glazov[10], I. Glushkov[37], L. Goerlich[6], M. Goettlich[11], N. Gogitidze[26], S. Gorbounov[37], C. Goyon[22], C. Grab[38], H. Grässler[2], T. Greenshaw[18], M. Gregori[19], G. Grindhammer[27], C. Gwilliam[21], D. Haidt[10], L. Hajduk[6], J. Haller[13], M. Hansson[20], G. Heinzelmann[11], R.C.W. Henderson[17], H. Henschel[37], O. Henshaw[3], G. Herrera[24], I. Herynek[31], R.-D. Heuer[11], M. Hildebrandt[34], K.H. Hiller[37], P. Höting[2], D. Hoffmann[22], R. Horisberger[34], A. Hovhannisyan[36], M. Ibbotson[21], M. Ismail[21], M. Jacquet[28], L. Janauschek[27], X. Janssen[10], V. Jemanov[11], L. Jönsson[20], D.P. Johnson[4], H. Jung[20,10], D. Kant[19], M. Kapichine[8], M. Karlsson[20], J. Katzy[10], N. Keller[39], I.R. Kenyon[3], C. Kiesling[27], M. Klein[37], C. Kleinwort[10], T. Klimkovich[10], T. Kluge[10], G. Knies[10], A. Knutsson[20], V. Korbel[10], P. Kostka[37], R. Koutouev[12], A. Kropivnitskaya[25], K. Krüger[14], J. Kückens[10], M.P.J. Landon[19], W. Lange[37], T. Laštovička[37,32], P. Laycock[18], A. Lebedev[26], B. Leißner[1], R. Lemrani[10], V. Lendermann[14], S. Levonian[10], L. Lindfeld[39], K. Lipka[37], B. List[38], E. Lobodzinska[37,6], N. Loktionova[26], R. Lopez-Fernandez[10], V. Lubimov[25], H. Lueders[11], D. Lüke[7,10], T. Lux[11], L. Lytkin[12], A. Makankine[8], N. Malden[21], E. Malinovski[26], S. Mangano[38], P. Marage[4], J. Marks[13], R. Marshall[21], M. Martisikova[10], H.-U. Martyn[1], S.J. Maxfield[18], D. Meer[38], A. Mehta[18], K. Meier[14], A.B. Meyer[11], H. Meyer[35], J. Meyer[10], S. Mikocki[6], I. Milcewicz-Mika[6], D. Milstead[18], A. Mohamed[18], F. Moreau[29], A. Morozov[8], J.V. Morris[5], M.U. Mozer[13], K. Müller[39], P. Murín[16,43], V. Nagovizin[25], K. Nankov[10], B. Naroska[11], J. Naumann[7], Th. Naumann[37], P.R. Newman[3], C. Niebuhr[10], A. Nikiforov[27], D. Nikitin[8], G. Nowak[6], M. Nozicka[32], R. Oganezov[36], B. Olivier[10], J.E. Olsson[10], D. Ozerov[25], C. Pascaud[28], G.D. Patel[18], M. Peez[29], E. Perez[9], D. Perez-Astudillo[23], A. Perieanu[10], A. Petrukhin[25], D. Pitzl[10], R. Plačakytė[27], R. Pöschl[10], B. Portheault[28], B. Povh[12], P. Prideaux[18], N. Raicevic[37], P. Reimer[31], A. Rimmer[18], C. Risler[10], E. Rizvi[19], P. Robmann[39], B. Roland[4], R. Roosen[4], A. Rostovtsev[25], Z. Rurikova[27], S. Rusakov[26], F. Salvaire[11], D.P.C. Sankey[5], E. Sauvan[22], S. Schätzel[13], J. Scheins[10], F.-P. Schilling[10], S. Schmidt[27], S. Schmitt[39], C. Schmitz[39], M. Schneider[22], L. Schoeffel[9], A. Schöning[38], V. Schröder[10], H.-C. Schultz-Coulon[14], C. Schwanenberger[10], K. Sedlák[31], F. Sefkow[10], I. Sheviakov[26], L.N. Shtarkov[26], Y. Sirois[29], T. Sloan[17], P. Smirnov[26], Y. Soloviev[26], D. South[10], V. Spaskov[8], A. Specka[29], B. Stella[33], J. Stiewe[14], I. Strauch[10], U. Straumann[39], V. Tchoulakov[8], G. Thompson[19], P.D. Thompson[3], F. Tomasz[14], D. Traynor[19], P. Truöl[39], G. Tsipolitis[10,40], I. Tsurin[10], J. Turnau[6], E. Tzamariudaki[27],

A. Uraev[25], M. Urban[39], A. Usik[26], D. Utkin[25], S. Valkár[32], A. Valkárová[32], C. Vallée[22], P. Van Mechelen[4], N. Van Remortel[4], A. Vargas Trevino[7], Y. Vazdik[26], C. Veelken[18], A. Vest[1], S. Vinokurova[10], V. Volchinski[36], B. Vujicic[27], K. Wacker[7], J. Wagner[10], G. Weber[11], R. Weber[38], D. Wegener[7], C. Werner[13], N. Werner[39], M. Wessels[1], B. Wessling[11], C. Wigmore[3], G.-G. Winter[10], Ch. Wissing[7], E.-E. Woehrling[3], R. Wolf[13], E. Wünsch[10], S. Xella[39], W. Yan[10], V. Yeganov[36], J. Žáček[32], J. Zálešák[31], Z. Zhang[28], A. Zhelezov[25], A. Zhokin[25], J. Zimmermann[27], H. Zohrabyan[36], and F. Zomer[28]

[1] *I. Physikalisches Institut der RWTH, Aachen, Germany*[a]
[2] *III. Physikalisches Institut der RWTH, Aachen, Germany*[a]
[3] *School of Physics and Astronomy, University of Birmingham, Birmingham, UK*[b]
[4] *Inter-University Institute for High Energies ULB-VUB, Brussels; Universiteit Antwerpen, Antwerpen; Belgium*[c]
[5] *Rutherford Appleton Laboratory, Chilton, Didcot, UK*[b]
[6] *Institute for Nuclear Physics, Cracow, Poland*[d]
[7] *Institut für Physik, Universität Dortmund, Dortmund, Germany*[a]
[8] *Joint Institute for Nuclear Research, Dubna, Russia*
[9] *CEA, DSM/DAPNIA, CE-Saclay, Gif-sur-Yvette, France*
[10] *DESY, Hamburg, Germany*
[11] *Institut für Experimentalphysik, Universität Hamburg, Hamburg, Germany*[a]
[12] *Max-Planck-Institut für Kernphysik, Heidelberg, Germany*
[13] *Physikalisches Institut, Universität Heidelberg, Heidelberg, Germany*[a]
[14] *Kirchhoff-Institut für Physik, Universität Heidelberg, Heidelberg, Germany*[a]
[15] *Institut für experimentelle und Angewandte Physik, Universität Kiel, Kiel, Germany*
[16] *Institute of Experimental Physics, Slovak Academy of Sciences, Košice, Slovak Republic*[f]
[17] *Department of Physics, University of Lancaster, Lancaster, UK*[b]
[18] *Department of Physics, University of Liverpool, Liverpool, UK*[b]
[19] *Queen Mary and Westfield College, London, UK*[b]
[20] *Physics Department, University of Lund, Lund, Sweden*[g]
[21] *Physics Department, University of Manchester, Manchester, UK*[b]
[22] *CPPM, CNRS/IN2P3 - Univ Mediterranee, Marseille - France*
[23] *Departamento de Fisica Aplicada, CINVESTAV, Mérida, Yucatán, México*[k]
[24] *Departamento de Fisica, CINVESTAV, México*[k]
[25] *Institute for Theoretical and Experimental Physics, Moscow, Russia*[l]
[26] *Lebedev Physical Institute, Moscow, Russia*[e]
[27] *Max-Planck-Institut für Physik, München, Germany*
[28] *LAL, Université de Paris-Sud, IN2P3-CNRS, Orsay, France*
[29] *LLR, Ecole Polytechnique, IN2P3-CNRS, Palaiseau, France*
[30] *LPNHE, Universités Paris VI and VII, IN2P3-CNRS, Paris, France*
[31] *Institute of Physics, Academy of Sciences of the Czech Republic, Praha, Czech Republic*[e,i]
[32] *Faculty of Mathematics and Physics, Charles University, Praha, Czech Republic*[e,i]
[33] *Dipartimento di Fisica Università di Roma Tre and INFN Roma 3, Roma, Italy*
[34] *Paul Scherrer Institut, Villigen, Switzerland*
[35] *Fachbereich C, Universität Wuppertal, Wuppertal, Germany*
[36] *Yerevan Physics Institute, Yerevan, Armenia*
[37] *DESY, Zeuthen, Germany*

[38] *Institut für Teilchenphysik, ETH, Zürich, Switzerland*[j]
[39] *Physik-Institut der Universität Zürich, Zürich, Switzerland*[j]

[40] *Also at Physics Department, National Technical University, Zografou Campus, GR-15773 Athens, Greece*
[41] *Also at Rechenzentrum, Universität Wuppertal, Germany*
[43] *Also at University of P.J. Šafárik, Košice, Slovak Republic*
[44] *Also at CERN, Geneva, Switzerland*
† *Deceased*

[a] *Supported by the Bundesministerium für Bildung und Forschung, FRG, under contract numbers 05 H1 1GUA /1, 05 H1 1PAA /1, 05 H1 1PAB /9, 05 H1 1PEA /6, 05 H1 1VHA /7 and 05 H1 1VHB /5*
[b] *Supported by the UK Particle Physics and Astronomy Research Council, and formerly by the UK Science and Engineering Research Council*
[c] *Supported by FNRS-FWO-Vlaanderen, IISN-IIKW and IWT and by Interuniversity Attraction Poles Programme, Belgian Science Policy*
[d] *Partially Supported by the Polish State Committee for Scientific Research, SPUB/DESY/P003/DZ 118/2003/2005*
[e] *Supported by the Deutsche Forschungsgemeinschaft*
[f] *Supported by VEGA SR grant no. 2/4067/24*
[g] *Supported by the Swedish Natural Science Research Council*
[i] *Supported by the Ministry of Education of the Czech Republic under the projects INGO-LA116/2000 and LN00A006, by GAUK grant no 173/2000*
[j] *Supported by the Swiss National Science Foundation*
[k] *Supported by CONACYT, México, grant 400073-F*
[l] *Partially Supported by Russian Foundation for Basic Research, grant no. 00-15-96584*

1 Introduction

Heavy quark production is an important process to study quantum chromodynamics (QCD). It is expected that perturbative QCD (pQCD) at next-to-leading order (NLO) should give a good description of heavy flavour production in deep-inelastic scattering (DIS), especially at values of the negative square of the four momentum of the exchanged boson Q^2 greater than the square of the heavy quark masses. Measurements of the open charm (c) cross section in DIS at HERA have mainly been of exclusive D or D^* meson production [1, 2]. From these measurements the contribution of charm to the proton structure function, $F_2^{c\bar{c}}$, is derived by correcting for the fragmentation fraction $f(c \to D)$ and the unmeasured phase space (mainly at low values of transverse momentum of the meson). The results are found to be in good agreement with pQCD predictions. The measurement of the beauty (b) cross section is particularly challenging since b events comprise only a small fraction (typically $< 5\%$) of the total cross section. The b cross section has been measured in DIS ($Q^2 > 2$ GeV^2) by ZEUS [3] and in photoproduction ($Q^2 \simeq 0$ GeV^2) by H1 [4] and ZEUS [5], using the transverse momentum distribution of muons relative to the b jet in semi-muonic decays. Measurements of the b cross section at high centre of mass energy have also been made in $p\bar{p}$ [6] and $\gamma\gamma$ collisions [7].

The analysis presented in this paper is of inclusive c and b cross sections in e^+p scattering at HERA in the range $Q^2 > 150$ GeV^2. Events containing heavy quarks can be distinguished from light quark events by the long lifetimes of c and b flavoured hadrons, which lead to displacements of tracks from the primary vertex. The distance of a track to the primary vertex is reconstructed using precise spatial information from the H1 vertex detector. The results presented in this paper are made in kinematic regions where there is little extrapolation needed to correct to the full phase space and so the model dependent uncertainty due to the extrapolation is small. The charm structure function $F_2^{c\bar{c}}$ and the corresponding structure function for b quarks $F_2^{b\bar{b}}$ are obtained after small corrections for the longitudinal structure functions $F_L^{c\bar{c}}$ and $F_L^{b\bar{b}}$. This is an extension to high Q^2 of previous H1 $F_2^{c\bar{c}}$ measurements and the first measurement of $F_2^{b\bar{b}}$.

2 Theory of Heavy Flavour Production in DIS

In pQCD, in the region where Q^2 is much larger than the squared mass M^2 of the heavy quark, the production of heavy flavour quarks is expected to be insensitive to threshold effects and the quarks may be treated as massless partons. At leading order (LO), in the 'massless' scheme, the quark parton model (QPM) process ($\gamma q \to q$) is the dominant contribution. At NLO, the photon gluon fusion ($\gamma g \to q\bar{q}$) and QCD Compton ($\gamma q \to qg$) processes also contribute. The approach is often referred to as the zero mass variable flavour number scheme (ZM-VFNS) [8, 9].

At values of $Q^2 \sim M^2$, the 'massive' scheme [10], in which the heavy flavour partons are treated as massive quarks is more appropriate. The dominant LO process is photon gluon fusion (PGF) and the NLO diagrams are of order α_s^2. The scheme is often referred to as the fixed flavour number scheme (FFNS). As Q^2 becomes large compared to M^2, the FFNS approach is unreliable due to large logarithms in $\ln(Q^2/M^2)$ in the perturbative series.

In order to provide reliable pQCD predictions for the description of heavy flavour production, over the whole range in Q^2, composite schemes which provide a smooth transition from the massive description at $Q^2 \sim M^2$ to the massless behaviour at $Q^2 \gg M^2$ have been developed [11, 12]. The scheme is commonly referred to as the variable flavour number scheme (VFNS). The approach has been incorporated in various different forms to order α_s [11] and to order α_s^2 [12].

3 H1 Detector

Only a short description of the H1 detector is given here; a full description may be found in [13]. A right handed coordinate system is employed at H1 that has its z-axis pointing in the proton beam, or forward, direction and x (y) pointing in the horizontal (vertical) direction.

Charged particles are measured in the central tracking detector (CTD). This device consists of two cylindrical drift chambers interspersed with z-chambers to improve the z-coordinate reconstruction and multi–wire proportional chambers mainly used for triggering. The CTD is situated in a uniform $1.15\,\mathrm{T}$ magnetic field, enabling momentum measurement of charged particles over the polar angular range $20^\circ < \theta < 160^\circ$ [1].

The CTD tracks are linked to hits in the vertex detector (central silicon tracker CST) [14], to provide precise spatial track reconstruction. The CST consists of two layers of double-sided silicon strip detectors surrounding the beam pipe, covering an angular range of $30^\circ < \theta < 150^\circ$ for tracks passing through both layers. This detector provides hit resolutions of 12 μm in r–ϕ and 25 μm in z. For CTD tracks with CST hits in both layers the transverse distance of closest approach (DCA) to the nominal vertex in x–y can be measured with a resolution of 33 $\mu\mathrm{m} \oplus 90$ $\mu\mathrm{m}/p_T[\mathrm{GeV}]$, where the first term represents the intrinsic resolution (including alignment uncertainty) and the second term is the contribution from multiple scattering in the beam pipe and the CST; p_T is the transverse momentum of the track.

The track detectors are surrounded in the forward and central directions ($4^\circ < \theta < 155^\circ$) by a fine grained liquid argon calorimeter (LAr) and in the backward region ($153^\circ < \theta < 178^\circ$) by a lead–scintillating fibre calorimeter [15] with electromagnetic and hadronic sections. These calorimeters provide energy and angular reconstruction for final state particles from the hadronic system. The LAr is also used in this analysis to measure and identify the scattered positron. An electromagnetic calorimeter situated downstream in the positron beam direction measures photons from the bremsstrahlung process $ep \to ep\gamma$ for the purpose of luminosity determination.

4 Experimental Method

The analysis is based on a high Q^2 sample of e^+p neutral current (NC) scattering events corresponding to an integrated luminosity of $57.4\ \mathrm{pb}^{-1}$, taken in the years 1999-2000, at an ep centre of mass energy $\sqrt{s} = 319\ \mathrm{GeV}$. The events are selected as described in [16]; the positron is

[1] The angular coverage of each detector component is given for the interaction vertex in its nominal position.

identified and measured in the LAr calorimeter, which restricts the sample to $Q^2 > 110\ \mathrm{GeV}^2$. The event kinematics, Q^2 and the inelasticity variable y, are reconstructed using the scattered positron. The Bjorken scaling variable x is obtained from $x = Q^2/sy$. After the inclusive selection the total number of events is around $121,000$.

4.1 Monte Carlo Simulation

The data are corrected for the effects of detector resolution, acceptance and efficiency by the use of Monte Carlo simulations. The Monte Carlo program RAPGAP [17] is used to generate high Q^2 NC DIS events for the processes $ep \to eb\bar{b}X$, $ep \to ec\bar{c}X$ and light quark production. RAPGAP combines $\mathcal{O}(\alpha_s)$ matrix elements with higher order QCD effects modelled by the emission of parton showers. The heavy flavour event samples are generated according to the massive PGF matrix element with the mass of the c and b quarks set to $m_c = 1.5\ \mathrm{GeV}$ and $m_b = 5.0\ \mathrm{GeV}$, respectively. The partonic system is fragmented according to the LUND string model implemented within the JETSET program [18]. The HERACLES program [19] calculates single photon radiative emissions off the lepton line and virtual electroweak corrections. In the event generation, the DIS cross section is calculated with a LO parton distribution function (PDF) [9]. In order to improve the description of the data by the simulation, the simulated inclusive cross section is reweighted in x and Q^2 using a NLO QCD fit (H1 PDF 2000) to the H1 data [16].

The samples of events generated for the uds, c and b processes are passed through a detailed simulation of the detector response based on the GEANT3 program [20], and through the same reconstruction software as is used for the data.

4.2 Track, Vertex and Jet Reconstruction

The analysis is based on CTD tracks which are linked to r–ϕ hits in both planes of the CST in order to improve the precision of the track parameters. In this paper, the CST-improved CTD tracks are referred to as 'CST tracks'. Only those events which have at least one reconstructed CST track with polar angle $30^\circ < \theta_{\mathrm{track}} < 150^\circ$ and a minimum transverse momentum of $0.5\ \mathrm{GeV}$ are used. At low values of y, the hadronic final state (HFS) tends to go forward and outside the acceptance of the CST. Therefore, the analysis is restricted to $0.07 < y < 0.7$. The upper y cut ensures a good trigger acceptance for the scattered positron. In this kinematic range, studies from Monte Carlo simulations show that 93% of c events and 96% of b events are expected to have at least one charged particle, with $p_T > 0.5\ \mathrm{GeV}$ in the angular range $30^\circ < \theta < 150^\circ$, produced from the decay of a c or b hadron. The extrapolation to the full phase space, needed to calculate $F_2^{c\bar{c}}$ and $F_2^{b\bar{b}}$, is therefore small.

The reconstructed z position of the interaction vertex must be within $\pm 20\ \mathrm{cm}$ of the centre of the detector to match the acceptance of the CST. The effect of the smearing of the z-vertex distribution around the nominal position reduces the number of selected events by $\sim 5\%$. The CST track reconstruction efficiency is 71% for a single charged particle with $p_T > 0.5\ \mathrm{GeV}$ that passes through the CST acceptance region. This efficiency includes the CST hit efficiency, CST-CTD linking efficiency and losses due to inactive CST regions. The polar angle and transverse

momentum distributions of HFS CST tracks are compared to the Monte Carlo simulation in figure 1. The simulation gives a reasonable description of these distributions.

The primary event vertex in r–ϕ is reconstructed from all tracks (with or without CST hits) and the position and spread of the beam interaction region (referred to as the 'beam-spot'). The beam-spot extension is measured to be $\sim 145\ \mu\mathrm{m}$ in x and $\sim 25\ \mu\mathrm{m}$ in y for the data period considered here. The position of the beam-spot is measured as the average over many events and the resulting error on the position is small in comparison to the size of the beam-spot, with a typical uncertainty of $\sim 5\ \mu\mathrm{m}$. The uncertainty on the primary event vertex for the kinematic range of this paper is on average $50\ \mu\mathrm{m}$ in x and $24\ \mu\mathrm{m}$ in y.

In this analysis the impact parameter, i.e. the transverse distance of closest approach of the track to the primary vertex point, is used to separate the different quark flavours (see section 4.3). The uncertainty of the measurement of the impact parameter receives contributions from the position of the primary vertex discussed above, the intrinsic resolution of the track and distortions due to multiple scattering in the beam-pipe and surrounding material. In order to provide a successful description of the data the Monte Carlo parameters for the beam-spot size, tracking resolution and detector material are adjusted to those observed in the data.

To identify long lived hadrons a 'jet axis' is defined for each event in order to calculate a signed impact parameter (δ) for each track. Jets with a minimum p_T of $5\ \mathrm{GeV}$, in the angular range $10^\circ < \theta < 170^\circ$, are reconstructed using the invariant k_T algorithm [21] in the laboratory frame using all reconstructed HFS particles. HFS particles are reconstructed using a combination of tracks and calorimeter energy deposits [22]. The jet axis is defined as the direction of the jet with the highest transverse momentum or, if there is no jet reconstructed in the event, as the 'direction of the struck quark in the quark parton model' [23] as reconstructed from the HFS particles. In the Q^2 range of this paper, the vector sum of all HFS particles in the laboratory frame always has a transverse momentum greater than $5\ \mathrm{GeV}$ and 97% of the events have the jet axis defined by a reconstructed jet.

CST tracks are associated to the jet axis if they lie within a cone of size 1 in pseudo-rapidity–ϕ space centred about the jet axis. Approximately 90% of those events with at least one HFS CST track have at least one CST track matched to the jet axis. Figure 2 shows the polar angle and p_T distributions of the jets which contain one or more CST tracks. Figure 3 shows the number of reconstructed CST tracks associated to the jet axis. The simulation gives a reasonable description of these distributions apart from at high multiplicities where the Monte Carlo is seen to lie a little below the data. The deviations are due to a non-perfect modelling of multiplicities in light quark jets and have a negligible effect on the measurements. The uncertainties on the heavy quark multiplicities and modelling are discussed in section 4.5.

4.3 Quark Flavour Separation

The different quark flavours that contribute to the DIS cross section are distinguished on the basis of the different lifetimes of the produced hadrons. Due to the relatively low cross sections and limited CST track reconstruction efficiency the decay length of the heavy hadrons is not reconstructed directly, but the impact parameter of tracks is used instead. The results, however, are checked by using an independent method based on the reconstruction of a secondary vertex

(see section 4.6). The chosen heavy flavour tagging method also allows events with only one CST track to be used, for which it is not possible to reconstruct a secondary vertex. For tracks associated to the jet axis, δ is defined as positive if the angle between the jet axis and the line joining the primary vertex to the point of DCA is less than 90°, and is defined as negative otherwise. Tracks from the decays of long lived particles will mainly have a positive δ. Tracks produced at the primary vertex result in a symmetric distribution around $\delta = 0$, i.e. negative δ tracks mainly result from detector resolution.

Figure 4(a) shows the δ distribution of CST tracks associated to the jet axis. The data are seen to be asymmetric with positive values in excess of negative values indicating the presence of long lived particles. The simulation gives a reasonable description of the data. The component of the simulation that arises from light quarks is almost symmetric at low δ. The asymmetry at $\delta \gtrsim 0.1$ cm is mainly due to long lived strange particles such as K^0_S. The c component exhibits a moderate asymmetry and the b component shows a marked asymmetry. The differences are due to the different lifetimes of the produced hadrons. In order to reduce the effects of the strange component, a cut of $|\delta| < 0.1$ cm is imposed on all tracks used in the analysis.

In order to optimise the separation of the quark flavours use is made of the significance, defined as the ratio of δ to its error. This distribution is shown for all tracks in figure 4(b), where a good description of the data by the simulation is observed apart from the tails. In the tails the data are observed to lie above the simulation, which is likely to be due to a non-perfect description of the resolution by the simulation. The differences in resolution between data and simulation are treated as a systematic error (see section 4.5).

A further optimisation is made by using different significance distributions for events with different multiplicities. The first significance distribution S_1 is defined for events where only one reconstructed CST track is linked to the jet, and is simply the significance of the track. The second significance distribution S_2 is defined for events with two or more tracks associated with the jet and is the significance of the track with the second highest absolute significance. Only events in which the tracks with the first and second highest absolute significance have the same sign are selected for the S_2 distribution. The second highest significance track is chosen because for heavy quarks ≥ 2 tracks are usually produced with high significance, whereas for light quarks the chances are small of two tracks being produced at large significance due to resolution effects. The S_1 and S_2 distributions are shown in figure 5. The distribution of S_2 gives a better separation power of light to heavy quarks. Events with one CST track are retained to improve the statistical precision of the measurements.

In order to substantially reduce the uncertainty due to the resolution of δ and the light quark normalisation the negative bins in the S_1 and S_2 distributions are subtracted from the positive. The subtracted distributions are shown in figure 6. It can be seen that the resulting distributions are dominated by c quark events, with an increasing b fraction with increasing significance. The light quarks contribute a small fraction for all values of significance.

4.4 Fit Procedure

The fractions of c, b and light quarks of the data are extracted in each x–Q^2 interval using a least squares simultaneous fit to the subtracted S_1 and S_2 distributions (as in figure 6) and the

total number of inclusive events before track selection. The c, b and uds Monte Carlo simulation samples are used as templates. Only the statistical errors of the data and Monte Carlo simulation are considered in the fit. The Monte Carlo c, b and uds contributions in each x–Q^2 interval are allowed to be scaled by factors P_c, P_b and P_l, respectively. The fit to the S_1 and S_2 distributions mainly constrains P_c and P_b, whereas the overall normalisation constrains P_l. The c and b quark fractions are distinguished in the fit by their different shapes in the S_1 and S_2 distributions.

The results of the fit to the complete data sample are shown in figure 6. The fit gives a reasonable description of the S_1 distribution and a good description of S_2 distribution, with a $\chi^2/n.d.f$ of $27.5/14$. Values of $P_c = 0.81 \pm 0.08$, $P_b = 1.62 \pm 0.24$ and $P_l = 1.05 \pm 0.02$ are obtained. Acceptable χ^2 values are also found for the fits to the samples in the separate x–Q^2 intervals.

Consistent results are found when fitting different significance distributions, for example fitting the S_1 or S_2 distributions alone; fitting the highest absolute significance track distribution for all events; fitting the distribution for the track with the third highest absolute significance, fitting the significance distributions without subtraction of the negative bins from the positive, and also when varying the range of significance to be fitted. The analysis was also repeated excluding the CST tracks associated to the jet axis from the primary vertex fit and compatible results were again found.

The results of the fit in each x–Q^2 interval are converted to a measurement of the differential c cross section using:

$$\frac{\mathrm{d}^2\sigma^{c\bar{c}}}{\mathrm{d}x\mathrm{d}Q^2} = \frac{\mathrm{d}^2\sigma}{\mathrm{d}x\mathrm{d}Q^2}\frac{P_c N_c^{\mathrm{MCgen}}}{P_c N_c^{\mathrm{MCgen}} + P_b N_b^{\mathrm{MCgen}} + P_l N_l^{\mathrm{MCgen}}}\delta_{\mathrm{BCC}}^{c\bar{c}}, \tag{1}$$

where $\mathrm{d}^2\sigma/\mathrm{d}x\mathrm{d}Q^2$ is the measured inclusive differential cross section from H1 [16] and N_c^{MCgen}, N_b^{MCgen} and N_l^{MCgen} are the generated number of c, b and light quark events from the Monte Carlo in each bin, respectively. A small bin centre correction $\delta_{\mathrm{BCC}}^{c\bar{c}}$ is applied using the NLO QCD expectation (see section 5) to convert the bin averaged measurement into a measurement at a single x–Q^2 point. The cross section is defined so as to include a correction for pure QED initial and final state radiative effects, but not electroweak corrections (see [16] for a more complete discussion). Events that contain c hadrons via the decay of b hadrons are not included in the definition of the c cross section. The structure function $F_2^{c\bar{c}}$ is then evaluated from the expression

$$\frac{\mathrm{d}^2\sigma^{c\bar{c}}}{\mathrm{d}x\mathrm{d}Q^2} = \frac{2\pi\alpha^2}{xQ^4}[(1+(1-y)^2)F_2^{c\bar{c}} - y^2 F_L^{c\bar{c}}], \tag{2}$$

where the longitudinal structure function $F_L^{c\bar{c}}$ is estimated from the NLO QCD expectation [16]. In the evaluation of $F_2^{c\bar{c}}$ the electroweak corrections are assumed to be small and are neglected. It is also convenient to express the cross section as a 'reduced cross section' defined as

$$\tilde{\sigma}^{c\bar{c}}(x,Q^2) = \frac{\mathrm{d}^2\sigma^{c\bar{c}}}{\mathrm{d}x\mathrm{d}Q^2}\frac{xQ^4}{2\pi\alpha^2(1+(1-y)^2)} = F_2^{c\bar{c}} - \frac{y^2}{1+(1-y)^2}F_L^{c\bar{c}}. \tag{3}$$

The differential b cross section and $F_2^{b\bar{b}}$ are evaluated in the same manner.

4.5 Systematic Errors

The systematic uncertainties on the measured cross sections are estimated by applying the following variations to the Monte Carlo simulation:

- A track efficiency uncertainty of 3% due to the CTD and of 2% due to the CST.
- An uncertainty in the δ resolution of the tracks (figure 4(a)) is estimated by varying the resolution by an amount that encompasses the differences between the data and simulation. An additional Gaussian smearing of $200\ \mu\mathrm{m}$ to 5% of randomly selected tracks and $25\ \mu\mathrm{m}$ to the rest is used.
- A 4% uncertainty on the hadronic energy scale.
- An error on the jet axis is estimated by introducing an additional Gaussian smearing of 2° in azimuth.
- The uncertainty on the asymmetry of the light quark δ distribution is estimated by repeating the fits with the light quark S_1 and S_2 distributions (figure 6) set to zero and doubling the contribution. This error includes the modelling of light quark multiplicities.
- The uncertainties on the various D and B meson lifetimes, decay branching fractions and mean charge multiplicities are estimated by varying the input values of the Monte Carlo simulation by the errors on the world average measurements, or by adjusting the simulation to the world average value depending on which variation is larger. For the branching fractions of b quarks to hadrons and the lifetimes of the D and B mesons the central values and errors on the world averages are taken from [24]. For the branching fractions of c quarks to hadrons the values and uncertainties are taken from [25]. For the mean charged track multiplicities the values and uncertainties for c and b quarks are taken from MarkIII [26] and LEP/SLD [27] measurements, respectively.
- An uncertainty on the fragmentation function of the heavy quarks is estimated using the Peterson fragmentation function [28] with parameters $\epsilon_c = 0.058$ and $\epsilon_b = 0.0069$.
- An uncertainty in the QCD model of heavy quark production is estimated by replacing the default RAPGAP model (where heavy quarks are generated with only the PGF process) with RAPGAP used with a $1:1$ ratio of QPM to PGF induced events.

Other sources of systematic error pertaining to the NC selection are also considered [16]: a 1.5% uncertainty on the luminosity measurement; an uncertainty on the scattered positron polar angle of 1–$3\ \mathrm{mrad}$ and energy of 0.7–3.0% depending on the polar angle; a 0.5% uncertainty on the scattered positron identification efficiency; a 0.5% uncertainty on the positron track-cluster link efficiency; a 0.3% uncertainty on the trigger efficiency and a 1% uncertainty on the cross section evaluation due to QED radiative corrections. An uncertainty due the bin centre correction is estimated to be 5%. This corresponds to the maximum correction for any x–Q^2 interval.

The uncertainties that contribute most to the total systematic error on $\tilde{\sigma}^{c\bar{c}}$ are the track resolution and the light quark δ asymmetry leading to errors on the cross section of 9% each.

Those that contribute most to the total systematic error on $\tilde{\sigma}^{b\bar{b}}$ are the track resolution, the track efficiency, and the QCD model leading to errors on the cross section of 14%, 11% and 8%, respectively. The total systematic error is obtained by adding all individual contributions in quadrature and is around 15% for $\tilde{\sigma}^{c\bar{c}}$ and 24% for $\tilde{\sigma}^{b\bar{b}}$. The same systematic error uncertainty is assigned to each of the four differential measurements.

4.6 Measurement Using Secondary Vertex Reconstruction

The results are checked using an alternative method to separate the quark flavours based on the explicit reconstruction of decay vertices in the transverse plane. In this approach, there is no definite assignment of tracks to vertices, but each track is assigned a weight with a range 0 to 1 for each vertex candidate, using the weight function of [29]. The larger the distance of the track to a vertex candidate, the smaller the weight. A simultaneous fit to a primary and a secondary vertex is made, with all tracks of the event considered for the primary vertex, whereas only tracks associated to the jet axis contribute to the secondary vertex. The vertex configuration that minimises the global fit χ^2 is found iteratively using deterministic annealing [30].

In the secondary vertex reconstruction analysis the same event, track and jet selections as applied in the impact parameter analysis are used. The number of tracks contributing with a weight greater than 0.8 to the secondary vertex, after the last annealing step, is used as a measure of the decay-multiplicity. The transverse distance between the primary and secondary vertex distributions L_{xy} for different decay-multiplicities is shown in figure 7. The vertices found in light quark events peak at $L_{xy} \simeq 0$, while the vertices found in heavy quark events are significantly displaced in the direction of the jet axis. Both charm and beauty decays contribute to the two track secondary vertex, whereas beauty dominates the three and four track secondary vertices.

When the L_{xy} distributions for the different multiplicities are fitted simultaneously using Monte Carlo templates for the c, b and uds quark contributions to obtain the scale factors P_c, P_b and P_l, the results are found to agree well with the impact parameter method. To illustrate this, the Monte Carlo contributions in figure 7 are scaled by the factors obtained using the impact parameter method.

5 Results

The measurements of $F_2^{c\bar{c}}$ and $F_2^{b\bar{b}}$ are listed in table 1 and shown in figure 8 as a function of x for two values of Q^2. The H1 data for $F_2^{c\bar{c}}$ are compared with the results of the ZEUS collaboration [2] where the cross sections were obtained from the measurement of $D^{*\pm}$ mesons. The results of the two measurements for $F_2^{c\bar{c}}$ are in good agreement.

The data are also compared with two example predictions from NLO QCD (see section 2). These are the H1 PDF 2000 fit [16] in which the c and b quarks are treated in the ZM-VFNS scheme, and a fit from MRST03 [31] which uses a VFNS scheme. The predictions of the two QCD approaches are similar and compatible with the data.

The measurements are also presented in table 2 and figure 9 in the form of the fractional contribution to the total ep cross section

$$f^{c\bar{c}} = \frac{\mathrm{d}^2\sigma^{c\bar{c}}}{\mathrm{d}x\mathrm{d}Q^2} / \frac{\mathrm{d}^2\sigma}{\mathrm{d}x\mathrm{d}Q^2}. \tag{4}$$

The b fraction $f^{b\bar{b}}$ is defined in the same manner. NLO QCD is found to give a good description of the data, as shown by comparison with the ZM-VFNS prediction from the H1 PDF 2000 fit.

The c and b fractions and cross sections are also measured integrated over the range $Q^2 > 150\ \mathrm{GeV}^2$ and $0.1 < y < 0.7$. This is a more restricted range than for the differential measurements in order that the acceptance for the scattered positron and products of the b and c quarks is above 95%, integrated across the kinematic range. The following values are found:

$$f^{c\bar{c}} = 0.183 \pm 0.019 \pm 0.023, \quad \sigma^{c\bar{c}} = 373 \pm 39 \pm 47\ \mathrm{pb},$$
$$f^{b\bar{b}} = 0.0272 \pm 0.0043 \pm 0.0060, \quad \sigma^{b\bar{b}} = 55.4 \pm 8.7 \pm 12.0\ \mathrm{pb}.$$

The integrated cross sections may also be compared with the predictions from NLO QCD. The VFNS prediction from MRST03 gives $\sigma^{c\bar{c}} = 426\ \mathrm{pb}$ and $\sigma^{b\bar{b}} = 47\ \mathrm{pb}$; the H1 PDF 2000 fit gives $\sigma^{c\bar{c}} = 455\ \mathrm{pb}$ and $\sigma^{b\bar{b}} = 52\ \mathrm{pb}$.

It is also useful to compare with results from the FFNS scheme, which was used for the QCD predictions in [3]. Using the PDF set CTEQ5F3 [32] gives $\sigma^{c\bar{c}} = 419\ \mathrm{pb}$ and $\sigma^{b\bar{b}} = 37\ \mathrm{pb}$. The values $m_c = 1.3\ \mathrm{GeV}$ and $m_b = 4.75\ \mathrm{GeV}$ were used and the renormalisation and factorisation scales were set to $\mu = \sqrt{p_{Tq\bar{q}}^2 + m_b^2}$, where $p_{Tq\bar{q}}$ is the mean transverse momentum of the heavy quark pair. Predictions for the cross sections may also be obtained from fits [33] to the HERA inclusive F_2 data based on CCFM evolution [34]. The CCFM predictions agree with those from the VFNS prediction of MRST03 to within 7%.

All the QCD predictions are observed to be compatible with the data. The errors on the data do not yet allow the different schemes to be distinguished. There is no evidence for a large excess of the b cross section compared with QCD predictions as has been reported in other measurements, which have been made in different kinematic ranges or for different processes [3, 4, 6, 7].

6 Conclusion

The inclusive charm and beauty cross sections in deep inelastic scattering are measured at high Q^2 using a technique based on the lifetime of the heavy quark hadrons. The measurements are made using all events containing tracks with vertex detector information. In the kinematic range of the measurements this eliminates the need for large model dependent extrapolations to the full cross section. Based on impact parameter measurements in the transverse plane both integrated and differential c and b cross sections are obtained. The results are verified using a method based on the explicit reconstruction of decay vertices. The cross sections and derived structure functions $F_2^{c\bar{c}}$ and $F_2^{b\bar{b}}$ are found to be well described by predictions of perturbative QCD. This is the first measurement of $F_2^{b\bar{b}}$.

Acknowledgements

We are grateful to the HERA machine group whose outstanding efforts have made this experiment possible. We thank the engineers and technicians for their work in constructing and maintaining the H1 detector, our funding agencies for financial support, the DESY technical staff for continual assistance and the DESY directorate for support and for the hospitality which they extend to the non-DESY members of the collaboration.

References

[1] C. Adloff *et al.* [H1 Collaboration], Z. Phys. C **72** (1996) 593 [hep-ex/9607012];
J. Breitweg *et al.* [ZEUS Collaboration], Phys. Lett. B **407** (1997) 402 [hep-ex/9706009];
C. Adloff *et al.* [H1 Collaboration], Nucl. Phys. B **545** (1999) 21 [hep-ex/9812023];
J. Breitweg *et al.* [ZEUS Collaboration], Eur. Phys. J. C **12** (2000) 35 [hep-ex/9908012];
C. Adloff *et al.* [H1 Collaboration], Phys. Lett. B **528** (2002) 199 [hep-ex/0108039].

[2] S. Chekanov *et al.* [ZEUS Collaboration], Phys. Rev. D **69** (2004) 012004 [hep-ex/0308068].

[3] S. Chekanov *et al.* [ZEUS Collaboration], Phys. Lett. B **599** (2004) 173 [hep-ex/0405069].

[4] C. Adloff *et al.* [H1 Collaboration], Phys. Lett. B **467** (1999) 156 [Erratum-ibid. B **518** (2001) 331] [hep-ex/9909029].

[5] J. Breitweg *et al.* [ZEUS Collaboration], Eur. Phys. J. C **18** (2001) 625 [hep-ex/0011081];
S. Chekanov *et al.* [ZEUS Collaboration], Phys. Rev. D **70** (2004) 012008 [hep-ex/0312057].

[6] F. Abe *et al.* [CDF Collaboration], Phys. Rev. Lett. **71** (1993) 2396;
F. Abe *et al.* [CDF Collaboration], Phys. Rev. D **53** (1996) 1051 [hep-ex/9508017];
S. Abachi *et al.* [D0 Collaboration], Phys. Rev. Lett. **74** (1995) 3548;
S. Abachi *et al.* [D0 Collaboration], Phys. Lett. B **370** (1996) 239.

[7] M. Acciarri *et al.* [L3 Collaboration], Phys. Lett. B **503** (2001) 10 [hep-ex/0011070].

[8] H. L. Lai *et al.*, Phys. Rev. D **55** (1997) 1280 [hep-ph/9606399].

[9] A. D. Martin, W. J. Stirling and R. G. Roberts, Phys. Rev. D **50** (1994) 6734 [hep-ph/9406315].

[10] E. Laenen, S. Riemersma, J. Smith and W. L. van Neerven, Nucl. Phys. B **392** (1993) 162;
E. Laenen, S. Riemersma, J. Smith and W. L. van Neerven, Nucl. Phys. B **392** (1993) 229;
S. Riemersma, J. Smith and W. L. van Neerven, Phys. Lett. B **347** (1995) 143 [hep-ph/9411431].

[11] F. I. Olness and W. K. Tung, Nucl. Phys. B **308** (1988) 813;

M. A. G. Aivazis, J. C. Collins, F. I. Olness and W. K. Tung, Phys. Rev. D **50** (1994) 3102 [hep-ph/9312319];

M. A. G. Aivazis, F. I. Olness and W. K. Tung, Phys. Rev. D **50** (1994) 3085 [hep-ph/9312318];

M. Krämer, F. I. Olness and D. E. Soper, Phys. Rev. D **62** (2000) 096007 [hep-ph/0003035];

S. Kretzer, H. L. Lai, F. I. Olness and W. K. Tung, Phys. Rev. D **69** (2004) 114005 [hep-ph/0307022];

R. S. Thorne and R. G. Roberts, Phys. Rev. D **57** (1998) 6871 [hep-ph/9709442];

R. S. Thorne and R. G. Roberts, Phys. Lett. B **421** (1998) 303 [hep-ph/9711223];

R. S. Thorne and R. G. Roberts, Eur. Phys. J. C **19** (2001) 339 [hep-ph/0010344];

M. Cacciari, M. Greco and P. Nason, JHEP **9805** (1998) 007 [hep-ph/9803400];

M. Cacciari, S. Frixione and P. Nason, JHEP **0103** (2001) 006 [hep-ph/0102134].

[12] M. Buza, Y. Matiounine, J. Smith and W. L. van Neerven, Phys. Lett. B **411** (1997) 211 [hep-ph/9707263];

A. Chuvakin, J. Smith and W. L. van Neerven, Phys. Rev. D **61** (2000) 096004 [hep-ph/9910250];

A. Chuvakin, J. Smith and W. L. van Neerven, Phys. Rev. D **62** (2000) 036004 [hep-ph/0002011].

[13] I. Abt *et al.* [H1 Collaboration], Nucl. Instrum. Meth. A **386** (1997) 310 and 348.

[14] D. Pitzl *et al.*, Nucl. Instrum. Meth. A **454** (2000) 334 [hep-ex/0002044].

[15] T. Nicholls *et al.* [H1 SPACAL Group Collaboration], Nucl. Instrum. Meth. A **374** (1996) 149.

[16] C. Adloff *et al.* [H1 Collaboration], Eur. Phys. J **C 30** (2003) 1 [hep-ex/0304003].

[17] H. Jung, Comput. Phys. Commun. **86** (1995) 147;
(see also http://www.desy.de/∼jung/rapgap.html).

[18] T. Sjöstrand, Comput. Phys. Commun. **82** (1994) 74.

[19] A. Kwiatkowski, H. Spiesberger and H. J. Möhring, Comput. Phys. Commun. **69** (1992) 155.

[20] R. Brun, R. Hagelberg, M. Hansroul and J. C. Lassalle, CERN-DD-78-2-REV.

[21] S. D. Ellis and D. E. Soper, Phys. Rev. D **48** (1993) 3160 [hep-ph/9305266];

S. Catani, Y. L. Dokshitzer, M. H. Seymour and B. R. Webber, Nucl. Phys. B **406** (1993) 187.

[22] C. Adloff *et al.* [H1 Collaboration], Z. Phys. C **74** (1997) 221 [hep-ex/9702003].

[23] T. Ahmed *et al.* [H1 Collaboration], Phys. Lett. B **298** (1993) 469.

[24] K. Hagiwara *et al.* [Particle Data Group Collaboration], Phys. Rev. D **66** (2002) 010001.

[25] L. Gladilin, "Charm hadron production fractions", hep-ex/9912064.

[26] D. Coffman *et al.* [MARK-III Collaboration], Phys. Lett. B **263** (1991) 135.

[27] D. Abbaneo *et al.* [LEP/SLD Heavy Flavour Working Group], LEPHF 2001-01; (available from http://lepewwg.web.cern.ch/LEPEWWG/heavy/)

[28] C. Peterson, D. Schlatter, I. Schmitt and P.M. Zerwas, Phys. Rev. D **27** (1983) 105.

[29] R. Frühwirth *et al.*, Nucl. Instrum. Meth. A **502** (2003) 699.

[30] R. Frühwirth and A. Strandlie, Comput. Phys. Commun. **120** (1999) 197.

[31] A. D. Martin, R. G. Roberts, W. J. Stirling and R. S. Thorne, Eur. Phys. J. C **35** (2004) 325 [hep-ph/0308087].

[32] H. L. Lai *et al.* [CTEQ Collaboration], Eur. Phys. J. C **12** (2000) 375 [hep-ph/9903282].

[33] M. Hansson and H. Jung, Proceedings of 11^{th} International Workshop on Deep Inelastic Scattering (DIS 2003), St. Petersburg, Russia, April 2003. Edited by V.T. Kim and L.N. Lipatov. p. 488 [hep-ph/0309009].

[34] M. Ciafaloni, Nucl. Phys. B **296** (1988) 49;

S. Catani, F. Fiorani and G. Marchesini, Phys. Lett. B **234** (1990) 339;

S. Catani, F. Fiorani and G. Marchesini, Nucl. Phys. B **336** (1990) 18;

G. Marchesini, Nucl. Phys. B **445** (1995) 49 [hep-ph/9412327].

x	y	Q^2 (GeV^2)	$\tilde{\sigma}^{c\bar{c}}$	$\delta^{c\bar{c}}_{\rm stat}$ (%)	$\delta^{c\bar{c}}_{\rm sys}$ (%)	$F_2^{c\bar{c}}$	$\tilde{\sigma}^{b\bar{b}}$	$\delta^{b\bar{b}}_{\rm stat}$ (%)	$\delta^{b\bar{b}}_{\rm sys}$ (%)	$F_2^{b\bar{b}}$
0.0050	0.394	200	0.197	17	15	0.202	0.0393	20	24	0.0413
0.0130	0.151	200	0.130	19	15	0.131	0.0212	29	24	0.0214
0.0130	0.492	650	0.206	22	15	0.213	0.0230	45	24	0.0243
0.0320	0.200	650	0.091	27	15	0.092	0.0124	37	24	0.0125

Table 1: The measured reduced NC charm ($\tilde{\sigma}^{c\bar{c}}$) and beauty ($\tilde{\sigma}^{b\bar{b}}$) cross sections, shown with statistical ($\delta^{c\bar{c}}_{\rm stat}$, $\delta^{b\bar{b}}_{\rm stat}$) and systematic ($\delta^{c\bar{c}}_{\rm sys}$, $\delta^{b\bar{b}}_{\rm sys}$) errors. The table also shows the values for $F_2^{c\bar{c}}$ and $F_2^{b\bar{b}}$ obtained from the measured cross sections using the NLO QCD fit to correct for $F_L^{c\bar{c}}$ and $F_L^{b\bar{b}}$.

x	y	Q^2 (GeV^2)	$f^{c\bar{c}}$	$\delta^{c\bar{c}}_{\rm stat}$ (%)	$\delta^{c\bar{c}}_{\rm sys}$ (%)	$f^{b\bar{b}}$	$\delta^{b\bar{b}}_{\rm stat}$ (%)	$\delta^{b\bar{b}}_{\rm sys}$ (%)
0.0050	0.394	200	0.181	17	15	0.0361	20	24
0.0130	0.151	200	0.163	19	15	0.0265	29	24
0.0130	0.492	650	0.239	22	15	0.0266	45	24
0.0320	0.200	650	0.150	27	15	0.0203	37	24

Table 2: The measured charm ($f^{c\bar{c}}$) and beauty ($f^{b\bar{b}}$) fractional contributions to the total cross section, shown with statistical ($\delta^{c\bar{c}}_{\rm stat}$, $\delta^{b\bar{b}}_{\rm stat}$) and systematic ($\delta^{c\bar{c}}_{\rm sys}$, $\delta^{b\bar{b}}_{\rm sys}$) errors.

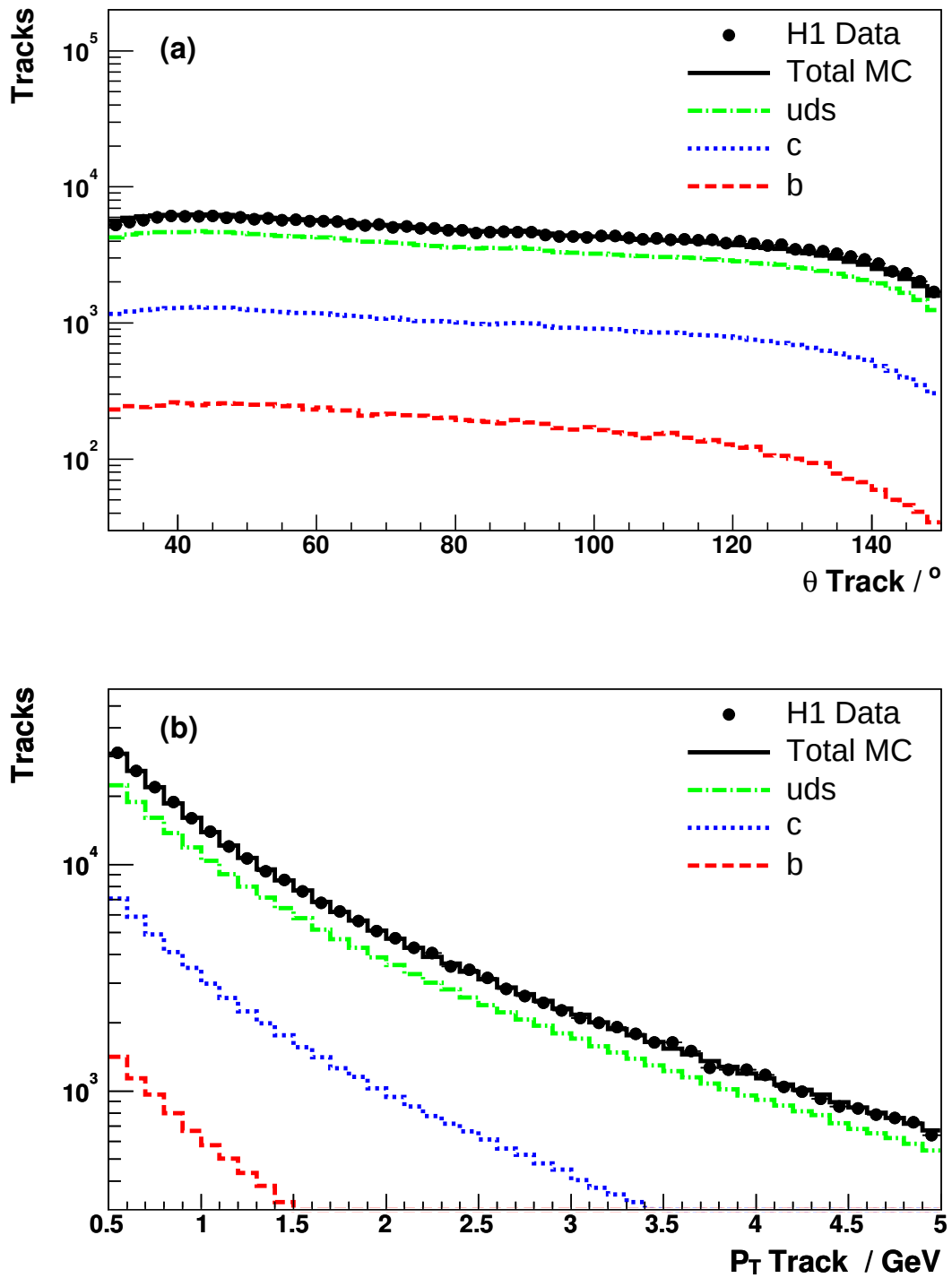

Figure 1: The polar angle distribution (a) and transverse momentum distribution (b) of all HFS CST tracks. Included in the figure is the expectation from the RAPGAP Monte Carlo simulation, showing the contributions from the various quark flavours after applying the scale factors obtained from the fit to the subtracted significance distributions of the data (see section 4.4).

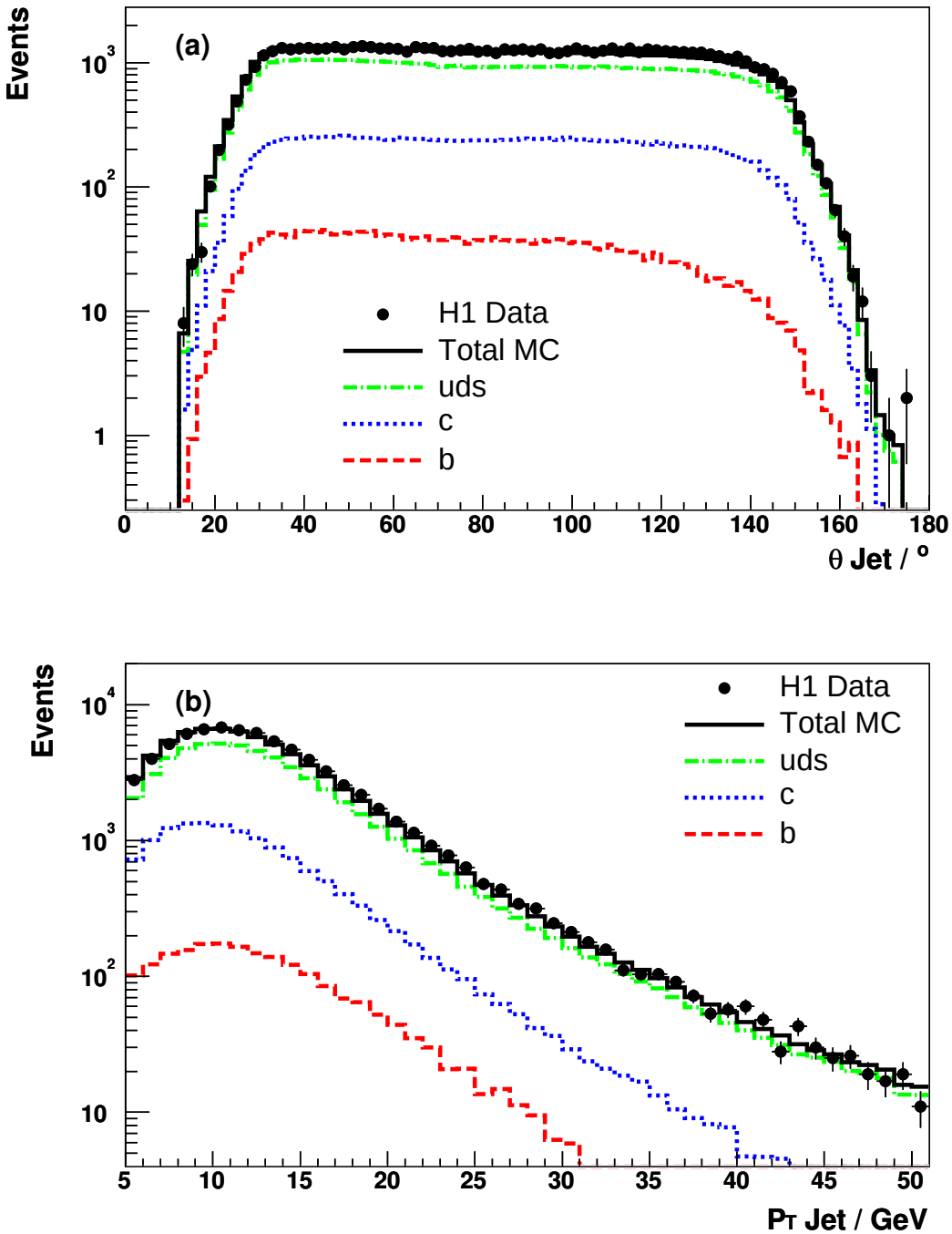

Figure 2: The polar angle distribution (a) and transverse momentum distribution (b) of the highest p_T jet which contains at least one reconstructed CST track within a cone of radius 1. If there are no reconstructed jets the complete hadronic final state is used to define the jet axis. Included in the figure is the expectation from the RAPGAP Monte Carlo simulation showing the contributions from the various quark flavours after applying the scale factors obtained from the fit to the subtracted significance distributions of the data.

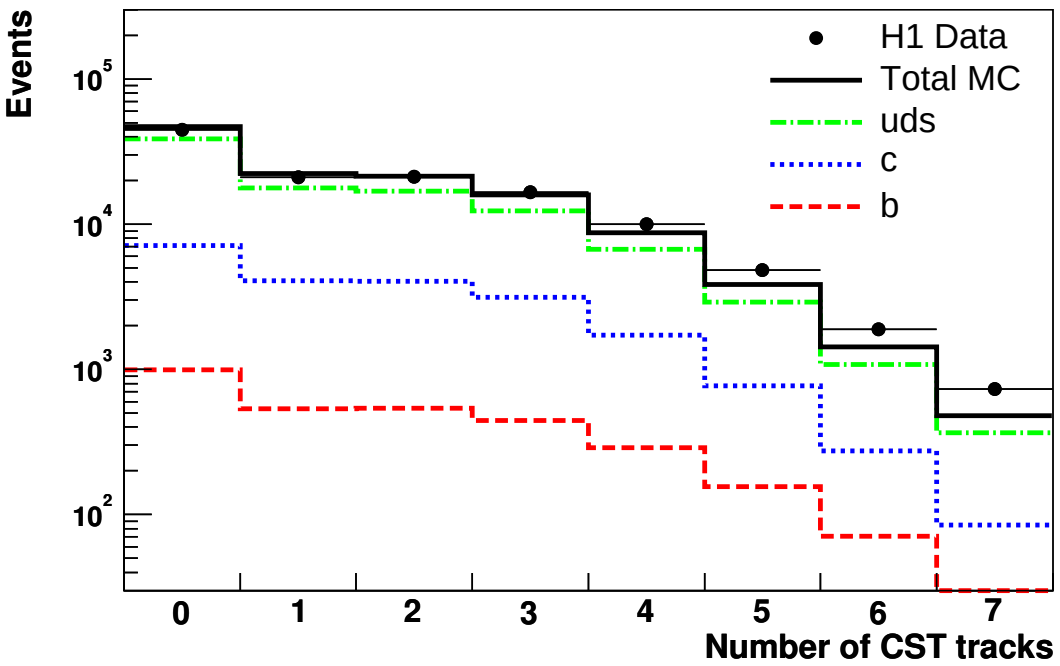

Figure 3: The number of reconstructed central silicon tracker (CST) tracks per event associated to the jet axis. Each CST track is required to have at least two CST hits and $p_T > 0.5$ GeV. Included in the figure is the expectation from the RAPGAP Monte Carlo simulation, showing the contributions from the various quark flavours after applying the scale factors obtained from the fit to the subtracted significance distributions of the data.

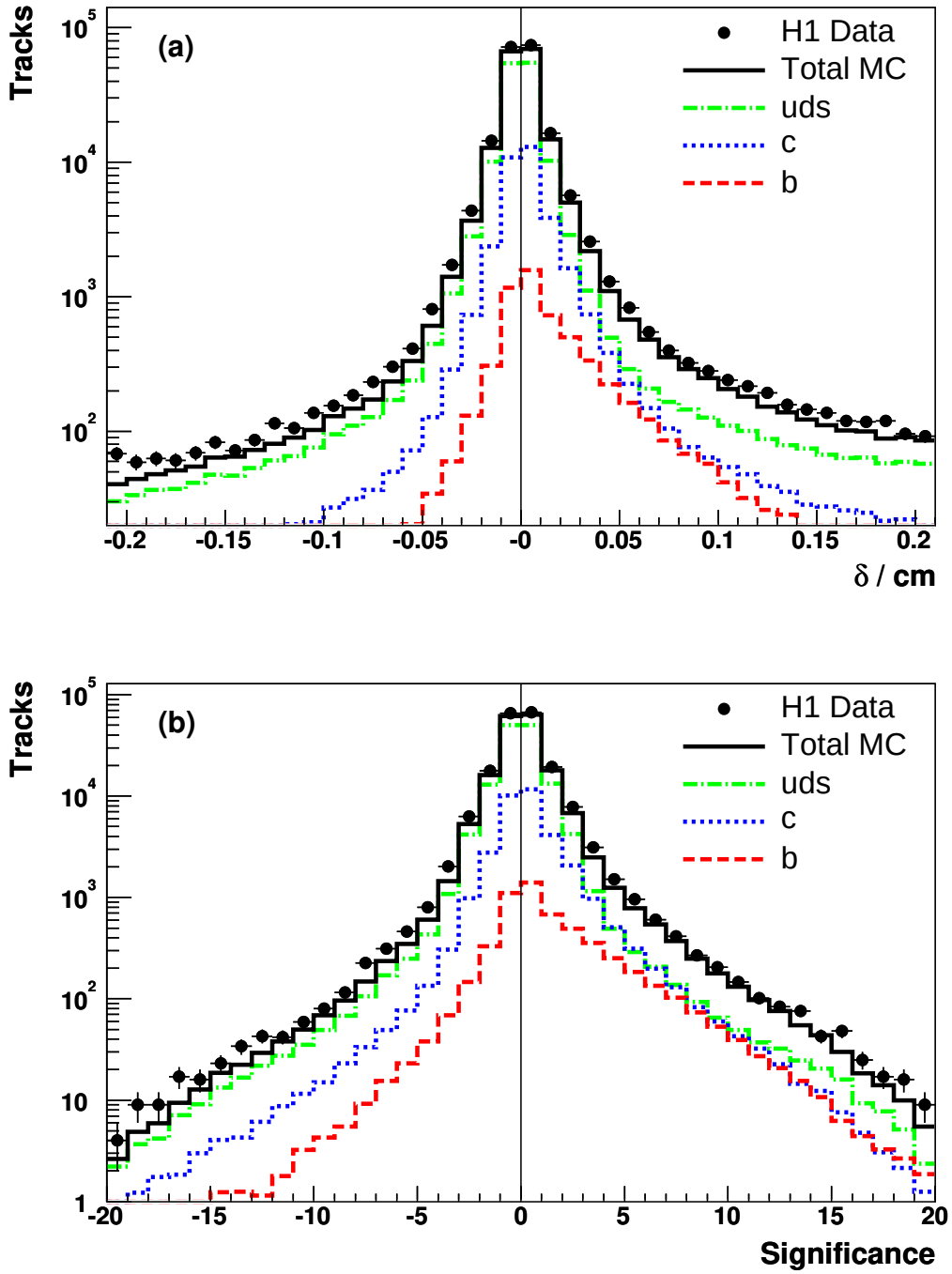

Figure 4: The signed impact parameter δ of a track to the primary vertex in the x–y plane (a) and the significance $\delta/\sigma(\delta)$ (b), where $\sigma(\delta)$ is the error on δ, for all CST tracks associated to the jet axis. The cut $|\delta| < 0.1$ cm has been applied in figure (b). Included in the figure is the expectation from the RAPGAP Monte Carlo simulation, showing the contributions from the various quark flavours after applying the scale factors obtained from the fit to the subtracted significance distributions of the data.

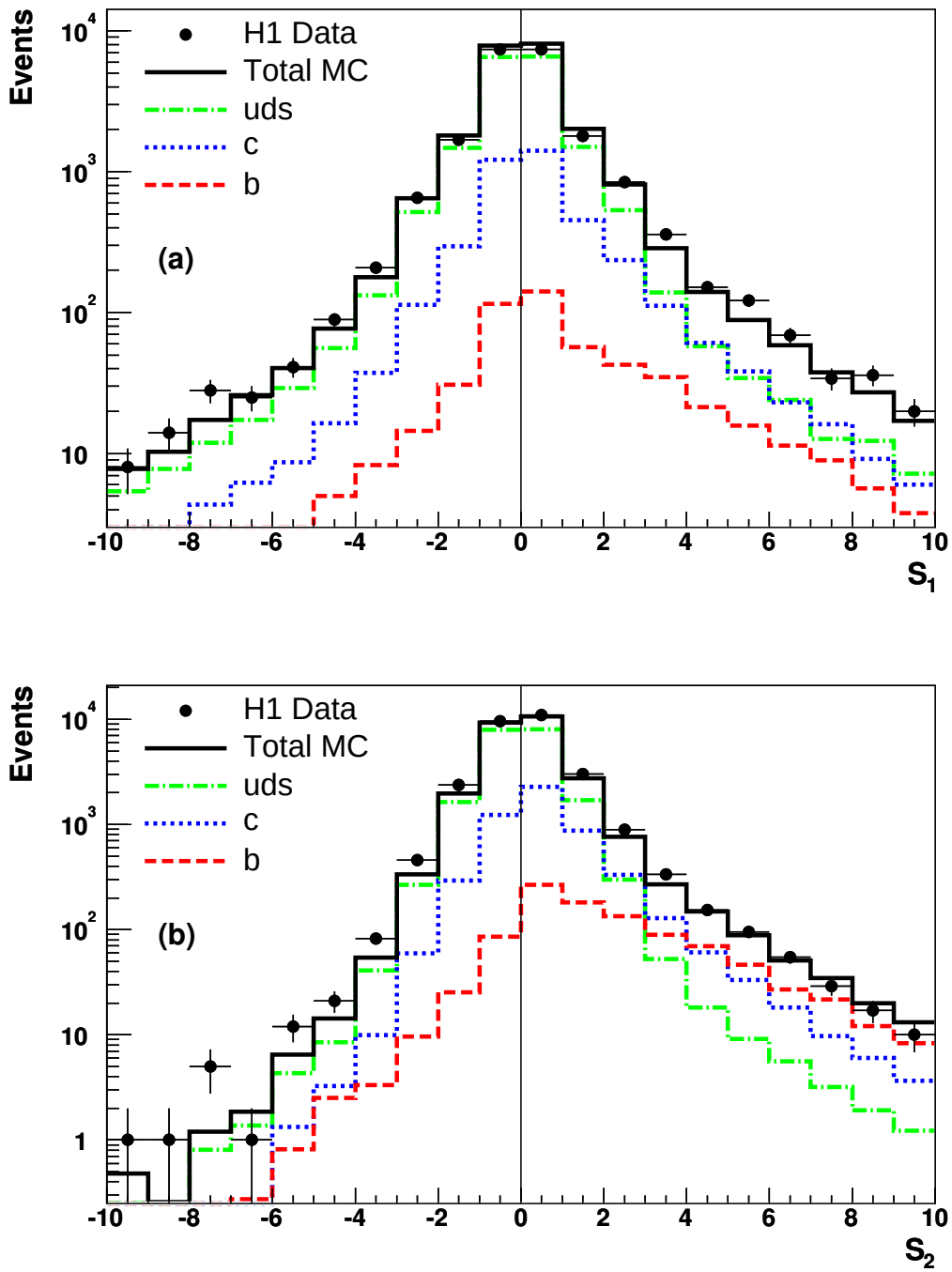

Figure 5: The significance $S_1 = \delta/\sigma(\delta)$ distribution per event (a) for events that contain one reconstructed CST track associated to the jet axis and the significance $S_2 = \delta/\sigma(\delta)$ distribution per event (b) of the track with the second highest absolute significance for events with ≥ 2 reconstructed CST tracks associated to the jet. Included in the figure is the expectation from the RAPGAP Monte Carlo simulation, showing the contributions from the various quark flavours after applying the scale factors obtained from the fit to the subtracted significance distributions of the data.

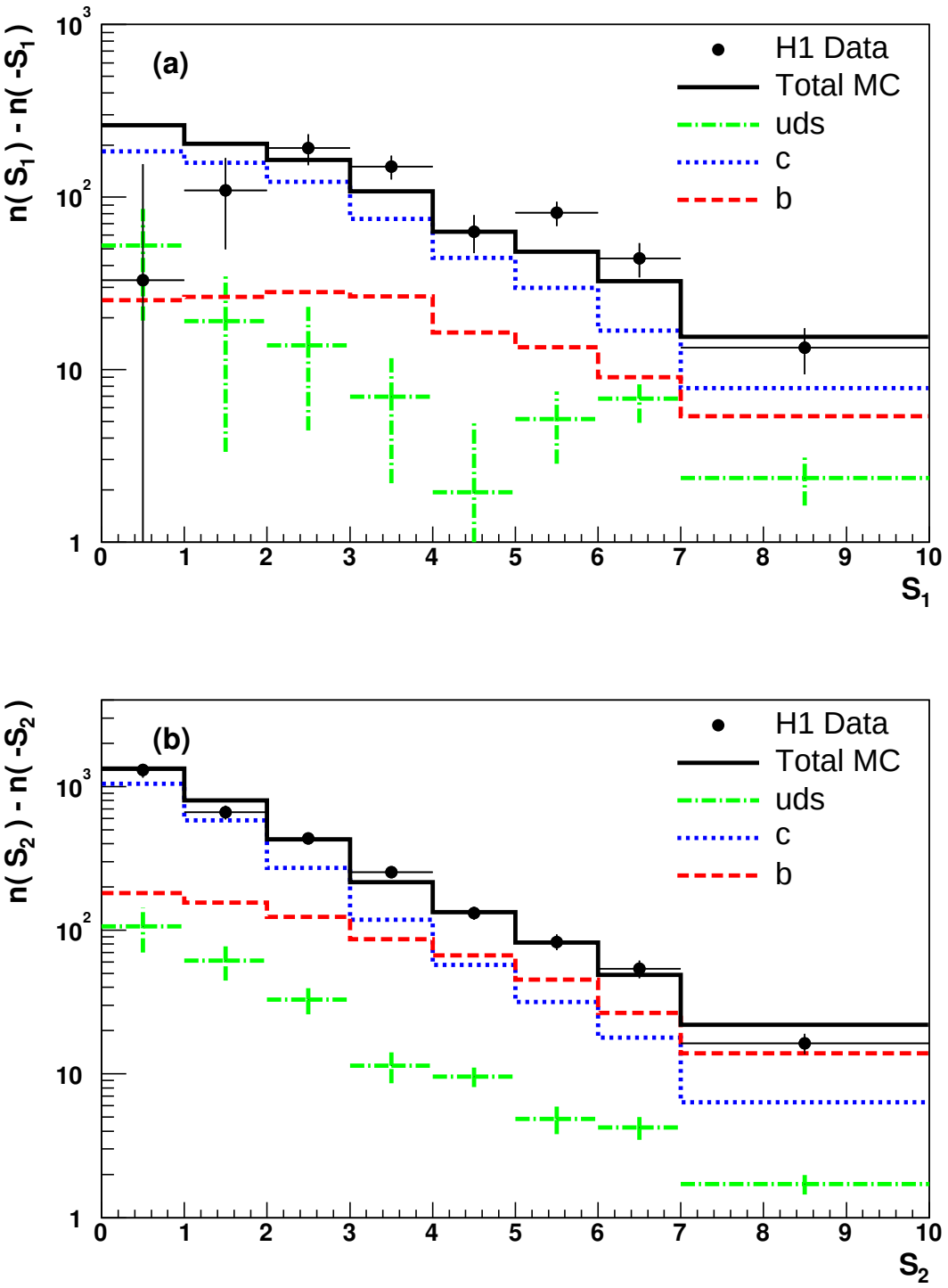

Figure 6: The subtracted distributions of (a) S_1 and (b) S_2. Included in the figure is the result from the fit to the data of the Monte Carlo distributions of the various quark flavours.

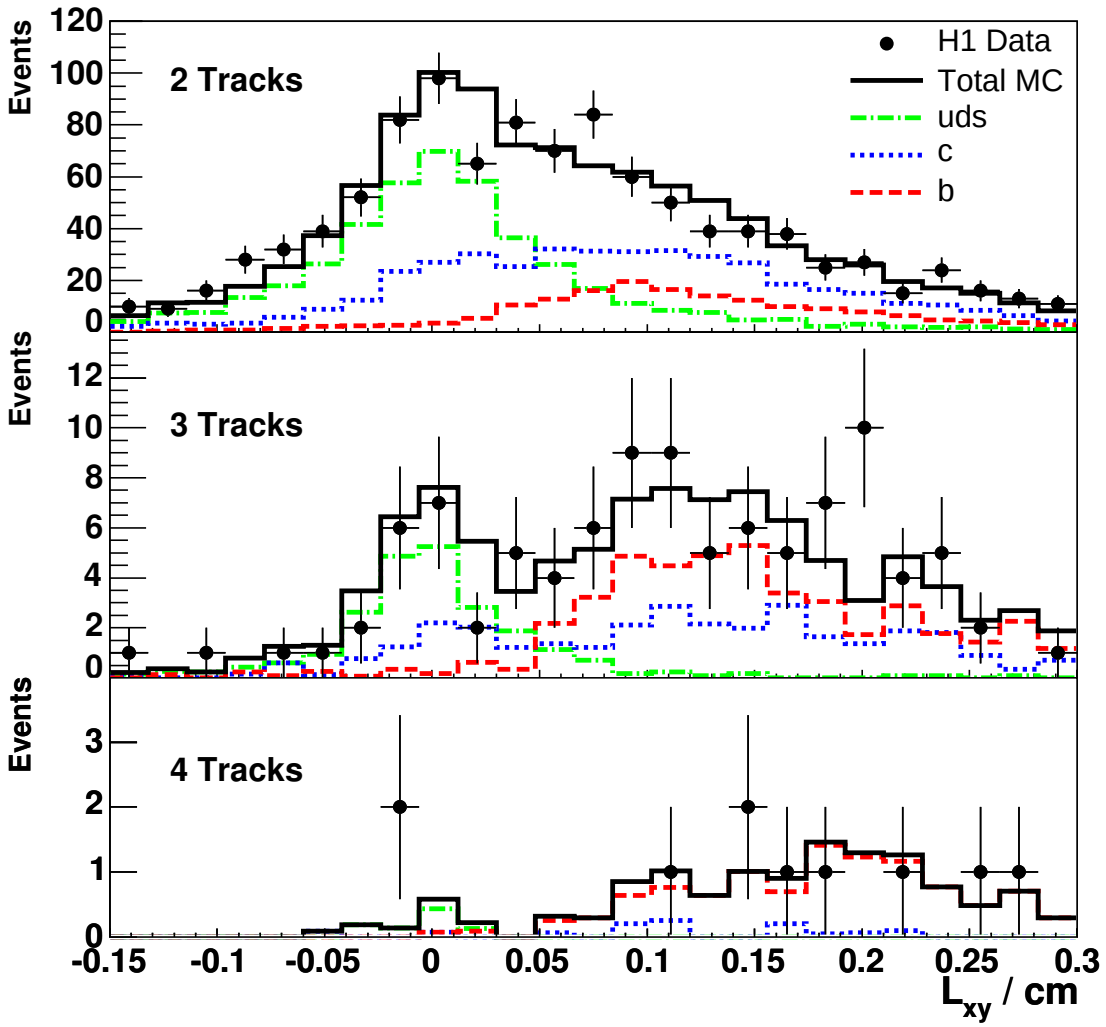

Figure 7: The transverse distance between the primary and secondary vertex (L_{xy}) for events with two, three and four CST tracks associated with the secondary vertex. Superimposed on the data points are c, b and light quark contributions that have been scaled by the results of the fit to the S_1 and S_2 data distributions.

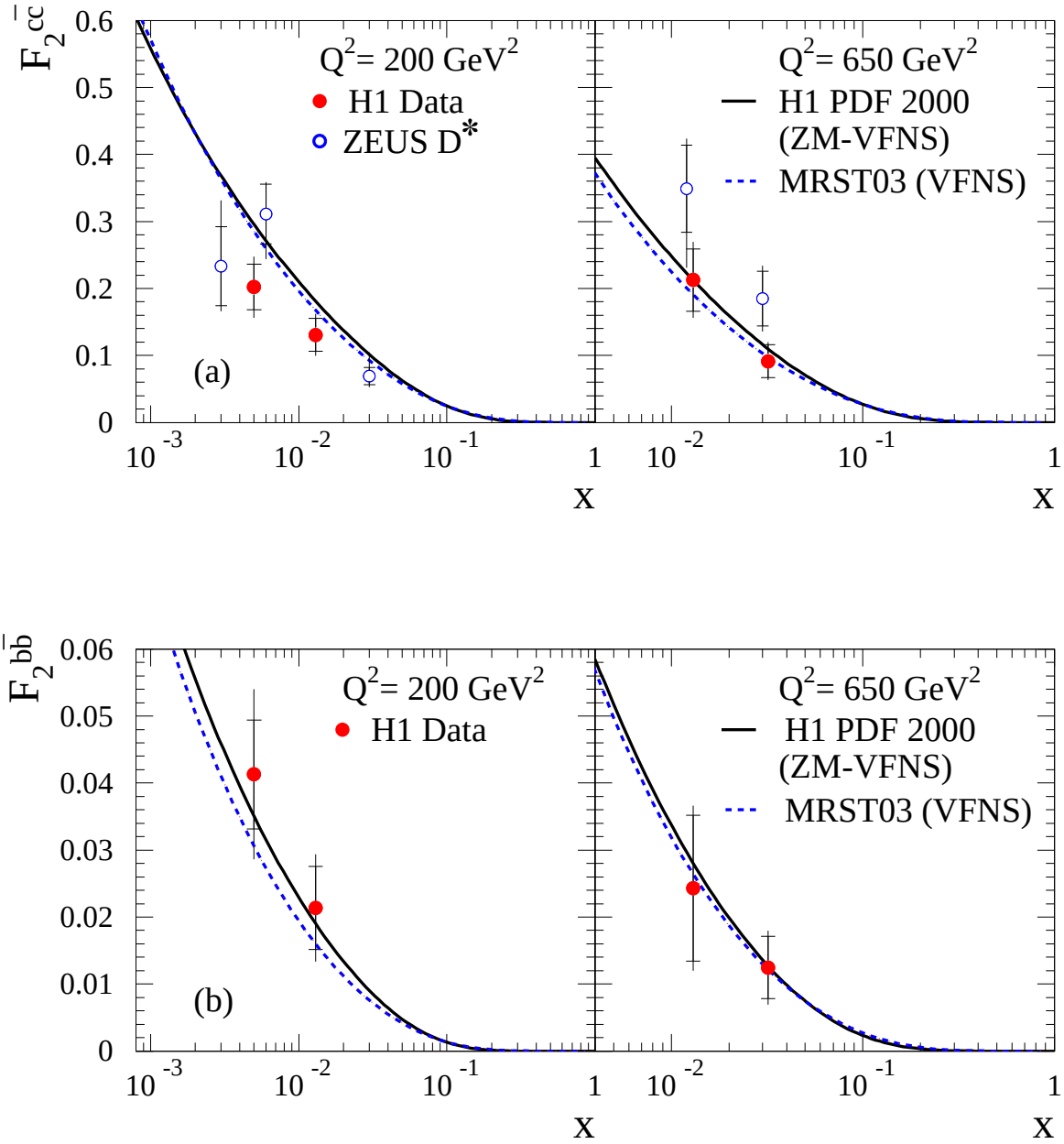

Figure 8: The measured $F_2^{c\bar{c}}$ (a) and $F_2^{b\bar{b}}$ (b) shown as a function of x for two different Q^2 values. The inner error bars show the statistical error, the outer error bars represent the statistical and systematic errors added in quadrature. The $F_2^{c\bar{c}}$ from ZEUS obtained from measurements of D^* mesons [2] and the predictions of NLO QCD fits [16, 31] are also shown.

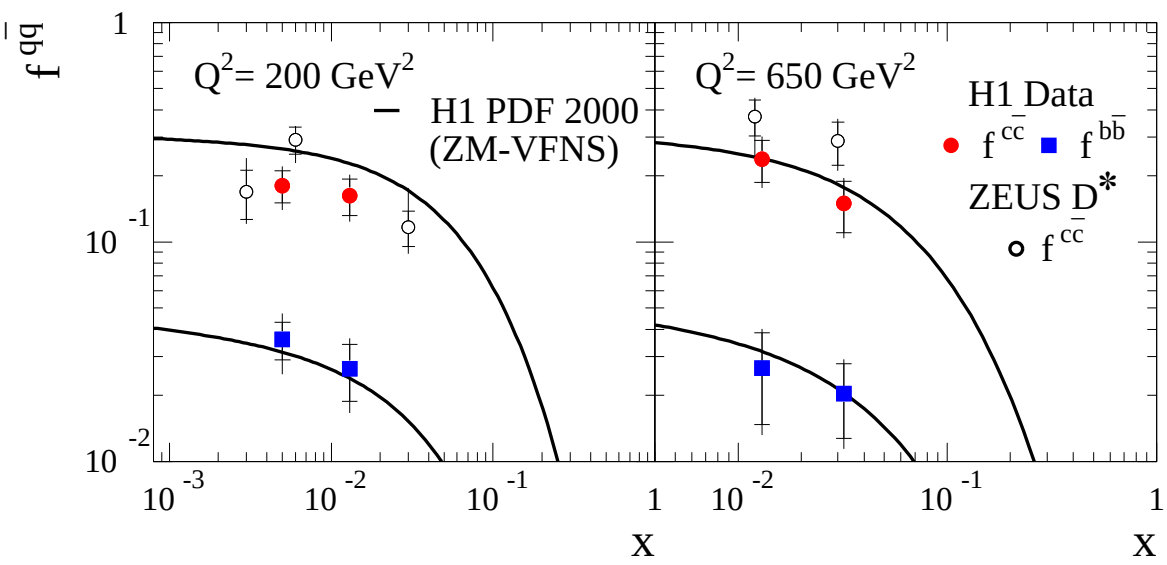

Figure 9: The contributions to the total cross section $f^{c\bar{c}}$ and $f^{b\bar{b}}$ shown as a function of x for two different Q^2 values. The inner error bars show the statistical error, the outer error bars represent the statistical and systematic errors added in quadrature. The $f^{c\bar{c}}$ from ZEUS obtained from measurements of D^* mesons [2] and the prediction of the H1 NLO QCD fit [16] are also shown.